Seasonal aspects of the recent pause in surface warming

Kevin E. Trenberth[1], John T. Fasullo[1], Grant Branstator[1] and Adam S. Phillips[1]
[1] National Center for Atmospheric Research, P.O. Box 3000, Boulder, CO 80307, USA
Nature Climate Change NCLIM-14050727

Factors involved in the recent pause in the rise of global mean temperatures are examined seasonally. For 1999 to 2012, the hiatus in surface warming is mainly evident in the central and eastern Pacific. It is manifested as strong anomalous easterly trade-winds, distinctive sea level pressure patterns, and large rainfall anomalies in the Pacific, which resemble the Pacific Decadal Oscillation (PDO). These features are accompanied by upper tropospheric teleconnection wave patterns that extend throughout the Pacific, to polar regions, and into the Atlantic. The extratropical features are particularly strong during winter. By using an idealized heating to force a comprehensive atmospheric model, the large negative anomalous latent heating associated with the observed deficit in central tropical Pacific rainfall is shown to be mainly responsible for the global quasi-stationary waves in the upper troposphere. The wave patterns in turn created persistent regional climate anomalies, increasing the odds of cold winters in Europe. Hence, tropical Pacific forcing of the atmosphere like that associated with a negative phase of the PDO produces many of the pronounced atmospheric circulation anomalies observed globally during the hiatus.

Although the 2000s are by far the warmest decade on record, the rate of increase of global mean temperature since 2000 has slowed, regardless of the data source[1], see Fig. 1 (and also Fig. S1 for northern winter aspects). A linear fit to the global mean temperatures after 1970 is quite good, and the biggest outlier is actually 1998, which was affected by substantial heat coming out of the ocean in association with the 1997/98 El Niño event[2,3]. Hence the post-1998 perspective (Fig. 1) is somewhat contrived because it depends on the choice of the starting year. Nevertheless it is vital to understand related interannual and decadal variability reflected in Fig. 1 and its regionality. The strongest pause in the rise in global mean surface temperatures is in the northern winter (Fig. S1), and the main places that warming has not occurred is in much of the central and eastern Pacific Ocean[1] and over northern continents, especially Eurasia[4]. Here we explore the teleconnections that are key to understanding the global structure of the various atmospheric anomalies associated with the warming hiatus, taking into account their seasonality to better determine the atmospheric forcings and responses, and understand the northern winter changes. This also provides an important perspective on the driving forces behind the patterns, and assists in discerning consequences from causes.

Several analyses of the factors involved in the apparent hiatus in the rise of global mean surface temperatures after about 2000 have been performed. Although small contributions have come from changes in the total solar irradiance as the sun has gone into a somewhat quieter phase since about 2004[5] and from aerosols in both the stratosphere (from small volcanic eruptions) and more regionally from pollution in the troposphere[6], more than half of the cause of the hiatus is apparently associated with internal climate variability[1,7,8,9] that we explore here.

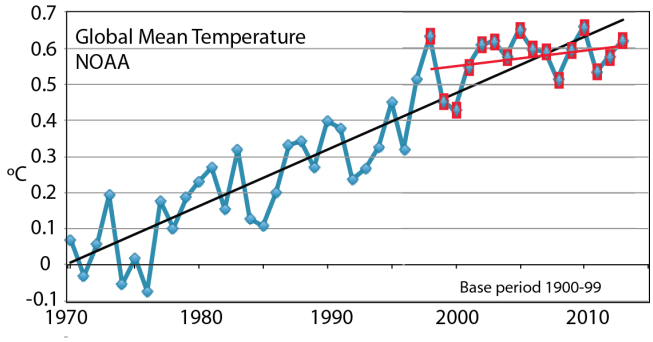

Figure 1 | Global mean surface temperature from NOAA, as anomalies relative to 1900–1999 plotted with linear trends for 1970–2013 (blue) and 1998–2013 (red).

Pacific decadal variability: seasonal signals

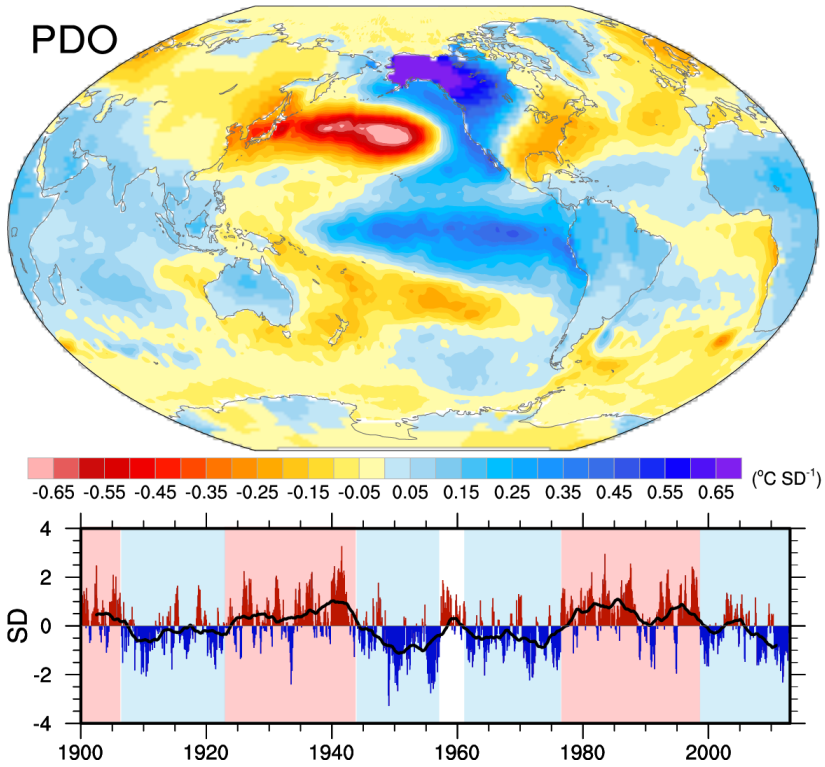

Figure 2 | The PDO based on an EOF analysis of SST anomalies with the global mean removed from 1900 to 2012 in the 20°–70° N 110° E–100° W region of the North Pacific, which explains 25% of the variance. The principal component time series, given below in normalized units, is regressed on global sea and land surface temperature anomalies to give the map above. The black curve is a 61-month running average. The light red and blue colours depict the positive and negative phases of the PDO. Note the reversal of the colour key in the top panel so that blue colours are positive, and hence the current negative phase has below-normal SSTs in the blue areas.

The phenomenon playing the main role is the PDO[1,9], alternatively known from a slightly different perspective as the Inter-decadal Pacific Oscillation (IPO), although it may not be a quasi-linear mode of natural variability[10]. The PDO was in a negative phase before 1976, but became positive from 1976 to 1998, a period coinciding with strong increases in global mean surface temperatures[11,1]. Then it switched to a negative phase in 1999 coinciding with the pause in upward trend in global mean surface temperatures. However, since 1999, the deeper ocean below 700m has taken up more heat and there has not been a reduction in the Earth's energy imbalance[8,3].

The PDO pattern (Fig. 2) emerges from an analysis of the departures from the global mean of Sea Surface Temperature (SST) monthly anomalies using a core region from 20 to 70°N 110°E to 100°W for an empirical orthogonal function analysis[11,1]. The base period is 1900 to 2012. The PDO/IPO has a Pacific-wide pattern in both surface and sub-surface temperatures with an El Niño-like pattern throughout the tropics and strong extratropical links in both hemispheres (see Fig. 2). The subsequent analysis only uses the PDO to provide markers for specifying the last two climate regimes: 1999-2012 versus 1976-1998[1]. This is more robust than using short-term linear trends[9], although results are similar. The recent PDO signals for the annual means[1] are complemented here with further diagnostic fields, including especially precipitation and atmospheric diabatic heating.

Since 1999 the annual mean tropical Pacific easterly trade winds have been much stronger than normal[1,9] (see also Fig. 3). In the tropics and sub-tropics this coincides with striking sea level pressure anomalies that relate to the Southern Oscillation. Much deeper warm waters have piled up in the western Pacific while cooler waters have prevailed through the top 500m in the eastern Pacific[1]. The result has been an increase in sea level of order 20 cm near the Philippines, but slight falls in the east since about 1999[12], accompanied by changes in Ocean Heat Content (OHC)[1].

The pronounced strengthening in Pacific trade winds in the 2000s was unprecedented after 1979 and not captured by 48 climate model projections[3,9] but was sufficient to account for the cooling of the tropical Pacific and a substantial slowdown in global surface warming through increased subsurface ocean heat uptake. While the strongest anomalies were indeed in the Pacific, strong connections also existed to the North Atlantic and southern oceans where subsurface ocean heat uptake penetrated to well below 700 m depth[1], altering surface winds and the distribution of Antarctic sea ice[13], and the winter

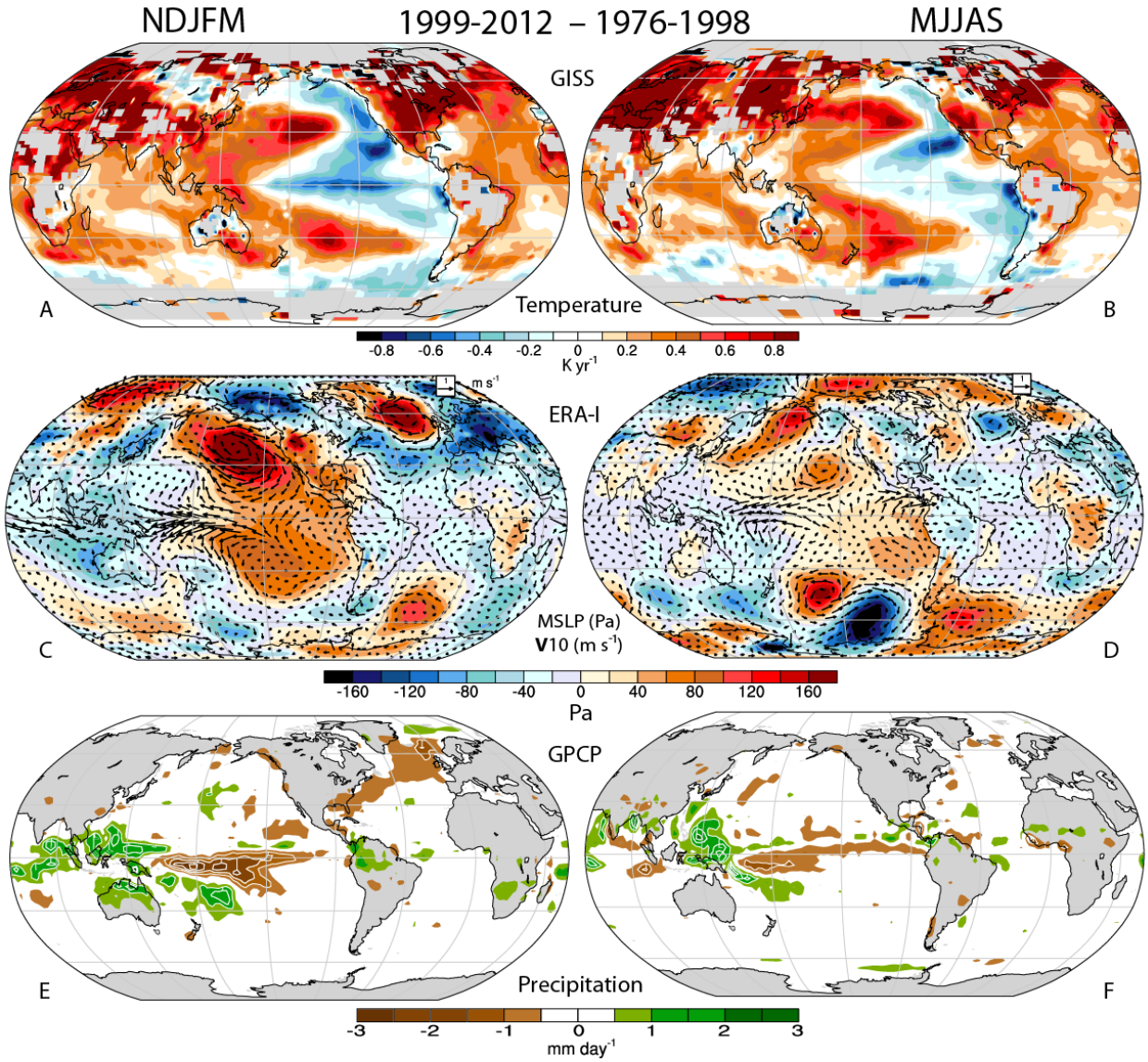

Figure 3 **a**–**f**, Mean differences between 1999–2012 and 1979–1998 for NDJFM (left) and MJJAS (right) for surface temperature from GISS (**a**,**b**), mean sea-level pressure (MSLP) differences from ERA-I (colours) and surface wind vectors (arrows) with the key at the top right (**c**,**d**), and precipitation from GPCP truncated to T63 resolution (**e**,**f**).

weather throughout Europe and North America. In the Pacific, the extra uptake came about through increased subduction in the Pacific shallow overturning cells, enhancing heat convergence in the equatorial thermocline[9,14,15].

Surface temperature (datasets are described in Supplementary Information (SI)) differences (Fig. 3A-B) clearly show that the central and eastern Pacific has failed to warm in the past 14 years, in a pattern associated with the PDO. To show the seasonality, two extended seasons November to March (NDJFM), northern winter, and May through September (MJJAS), northern summer, are examined. The Pacific cooling is stronger in northern winter (Fig. 3A). In general, surface warming deviates considerably from the PDO pattern outside of the Pacific basin, perhaps signaling a substantial role for external forcing of the climate system and other factors such as internal variability beyond that associated with the PDO.

Precipitation differences between these two regimes (Fig. 3E-F) feature patterns similar to those associated with La Niña: much drier from 160°E to South America along the equator, a northward shifted but weaker northern Intertropical Convergence Zone (ITCZ), a southwestward shifted South Pacific Convergence Zone (SPCZ), and extensive heavy rains over the Indonesian maritime continent. Wet conditions over northern Australia, Southeast Asia, northern Brazil, Colombia and Venezuela, extend over the tropical Indian and Atlantic Oceans (SI Fig. S2) and are likely associated with changes in the Walker Circulation[16]. The subtropical Pacific dry zone extends across the southeastern United States and throughout

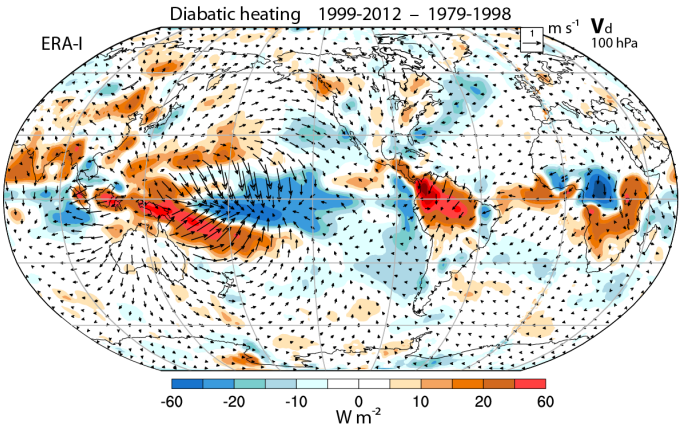

Figure 4 | Vertically integrated diabatic heating computed as a residual from the energy equation and lightly smoothed with a 4-point smoother, plus the divergent wind component at 100 hPa for the difference between 1999–2012 and 1979–1998 for the annual means, based on ERA-I reanalyses.

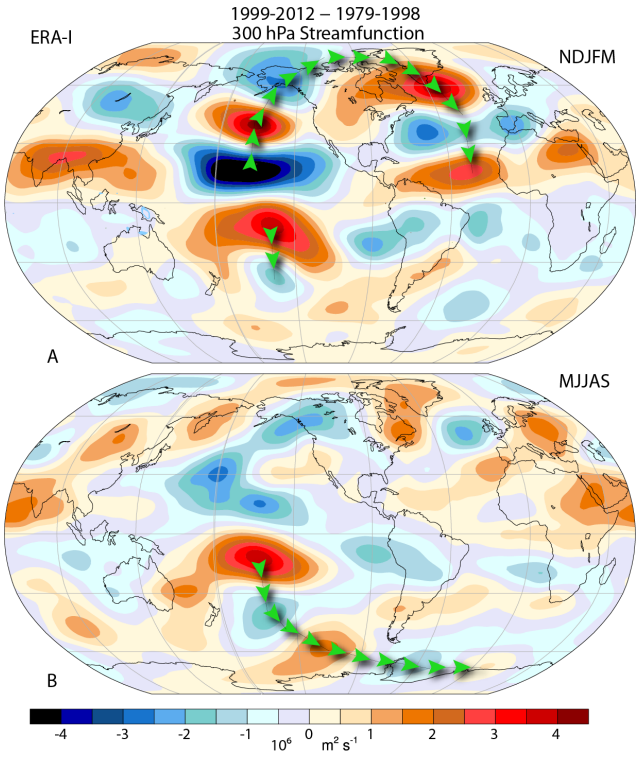

Figure 5 | The streamfunction at 300 hPa for the diferences between 1999–2012 and 1979–1998 for NDJFM and MJJAS. The rotational wind is parallel to the contours. The green arrowheads show schematically the main wave trains emanating from the tropical Pacific.

much of the North Atlantic in winter. Considering that the differences in Fig. 3 are for a 14-year period, the extent of the values exceeding 1 mm day^{-1} is exceedingly large (p <0.05 based on the interannual standard deviation in the tropical Pacific from 1979-1995[17] and two-sided Student's t-test), and suggests that much greater values occur in some years.

Complementary perspectives provided by the changes in sea level pressure and surface winds (Fig. 3C-D) have some similarity in the tropical Pacific in both seasons, with a positive Southern Oscillation index, but exhibit stronger anomalies in NDJFM. In the tropics, the intensification of easterly winds just south of the equator near the dateline in NDJFM exceeds 2 m s^{-1} versus about 1.1 m s^{-1} in MJJAS. These compare with mean vector wind speeds of up to 8 m s^{-1} in DJF and less than 7 m s^{-1} in JJA for 1950-79[18]. Seasonal mean standard deviations are mostly less than 1 m s^{-1}, and hence an anomaly of 1 m s^{-1} over 14 years is highly statistically significant (p <0.01). Sea level pressure anomalies are large in both hemispheres in the subtropics, but stronger somewhat wave-like teleconnections in each hemisphere occur in winter.

The regime differences for the diabatic heating from radiation and latent and sensible heating of the atmosphere (Fig. 4) have been computed as a residual of the energy equations using ERA-I data[19,20]. Because 1 mm day^{-1} is equivalent to latent heating of about 29 W m^{-2}, its dominant role in the anomalous diabatic heating is apparent from comparing Figs. 3E, F with Fig. 4, and it is where precipitation anomalies exceed at least 0.5 mm day^{-1} over broad areas that a significant decadal response in terms of atmospheric teleconnections can be expected[21,22].

The degree to which the extratropical signal is wave-like in sea level pressure is better seen in a polar projection (Fig. S3). The alternating anomalies are clearest in MJJAS in the southern hemisphere. However, wave-like responses are best seen in the upper troposphere in the streamfunction field. Accordingly, we focus on the 300 hPa streamfunction differences (Fig. 5), which depict the rotational part of the flow (the flow is along the contours). By far the strongest feature is the dipole structure in the central tropical Pacific straddling both the equator and the region of the strongest precipitation deficit. There is a single predominant center in the upper tropospheric tropics of each hemisphere with a cyclonic sign, as expected in conjunction with strong meridional convergence into the equatorial region and subsidence[21] which can be inferred from the divergent wind components at 100 hPa (Fig. 4). That convergence is consistent with local atmospheric overturning driven by precipitation latent heat anomalies. The negative heating anomalies associated with the exceptionally dry tongue along the equator evidently dominate the atmospheric forcing (Fig. 4). The pattern outside the tropics is strongly suggestive of a wave-train of Rossby waves emanating from these regions, that are strongest in winter[21], as indicated schematically by the green arrows. This pattern constructively interferes with the observed long-term trend in tropospheric circulation[23] in some regions, and destructively in others.

From theory and modeling[21,22], tropical SST anomalies in the central and western Pacific are very effective in driving robust extratropical atmospheric responses. High SST anomalies lead to low surface pressure and low-level moisture convergence that feeds high precipitation, and vice versa for

low SST anomalies. The latent heat (Figs. 3E-F) release in turn drives overturning circulations brought about in part by anomalous Walker circulations (Figs. 4; 5) throughout the tropics, and forces extratropical Rossby waves via the anomalous upper level divergence flow (Fig. 4) perhaps involving the lower stratosphere[24] in the extratropics. The term $\beta v'_d$ in the atmospheric vorticity equation, where β is the meridional gradient of the Coriolis parameter and v'_d is the anomalous divergent northerly wind component (see SI), makes a large contribution to driving the changes in the rotational flow[19,25] owing to the large values of v'_d (Fig. 4).

The stationary Rossby waves tend to follow a great circle route, and in turn alter the mid-latitude storm tracks, transient eddy heat and momentum transports, and interact with orography and the climatological mean flow. Negative SST anomalies and associated local precipitation deficits tend to have effects of opposite sign.

Idealized model simulations of response

A climate model driven with specified observed PDO-related SSTs in the tropical central and eastern Pacific but freely coupled elsewhere[7] replicated many atmospheric features associated with the PDO, including an enhanced Walker circulation and several seasonal aspects, although it also missed many important details of the summer precipitation anomalies (which was the only season presented) although it did capture the drying over the U.S. Influences over the Atlantic, Arctic and Europe were not picked up.

To further provide evidence that the global response originates in the tropics, we have carried out several idealized experiments with the NCAR Community Atmospheric Model version 3 (CAM3); see SI for details. Imposed heating (positive or negative) over a circle of half-amplitude radius of 750 km is placed on the equator in runs that otherwise have climatological SSTs that vary only with day of year. The experiments have been run for 20 years, which is long enough for robust results, and compared to the mean climate of a 200-year control integration.

The model response varies with season. Results for cooling anomalies imposed on the equator at 180° for NDJFM and at 165°W for MJJAS (Fig. 6), meant to mimic rainfall deficits, show the same seasonality seen in observations, with global upper tropospheric wave-trains being preferentially generated in the winter hemisphere of each season (Fig. 5). Moreover, many of the individual observed anomalies are also reproduced in the experiment, even as far away as the North and South Atlantic. The heating position does not make a substantial contribution to the seasonality of the response. Because SSTs are imposed, some of the heat is dispersed into the ocean, while the rest is radiated to space at higher latitudes. Not only does this process force the planetary-scale waves, but the storm tracks are also altered and feedback onto the planetary waves through transient eddy heat and momentum fluxes to produce the final result. We have imposed a monopole of negative heating in the experiments while in the observations there is compensating heating at other longitudes. As a simple way to approximate its influence, we have removed the zonal mean (Fig. 6). The equivalent plot with the zonal mean included shows a more complex response, especially in the northern hemisphere for NDJFM (Fig. S4).

Some studies have emphasized the western tropical Pacific as an effective region for forcing midlatitudes[26-28], but we find for the hiatus that the central tropical Pacific is likely the dominant source region. A significant response to western Pacific heating would produce an upper tropospheric subtropical anticyclone but there is none in the hiatus pattern, consistent with the weak anomalous divergence in that region (Fig. 4). Moreover, CAM3 experiments (not shown) with idealized heating in the western Pacific do not produce a mid-latitude response that matches the mid-latitude hiatus pattern.

Although our experiments are idealized they include the key complex interactions within the atmosphere that occur in nature in the response, and serve to demonstrate certain properties of the climate system, but they are not intended to be a comprehensive simulation. Rather their merit lies in their simplicity and how well the results agree with observations. They strongly support the earlier interpretation that many of the atmospheric anomalies observed during the hiatus (Fig. 5) are likely forced from the tropics by the ocean.

The cause for the pause

Our results suggest that the hiatus in global mean temperature rise has been strongly influenced by the negative phase of the PDO. The planet is still warming[8], but the changes in atmospheric circulation and surface winds, in particular, have changed ocean currents and more heat is being sequestered at greater depths. Effects are greatest in northern winter and there are profound regional manifestations. In particular, a cooler Europe is not reflected in the regime shift patterns in Fig. 3A, and instead was related to a trend within the past epoch and cooler years after 2005 in winter[4,1]; see Fig. S1. In northern winter, teleconnections via quasi-stationary atmospheric Rossby waves forced from the tropical Pacific influenced the Arctic and predisposed the North Atlantic Oscillation (NAO) to be in its negative phase (Figs. 3C, 5A, 6A). In turn this favors cold outbreaks in Europe, as occurred in 2009-10, 2010-11, and 2012-13 (Fig. S5). These results help explain why the main absence of very recent warming over land has been over Eurasia in winter[4,1].

When atmospheric circulation patterns persist then there is generally anomalous atmospheric forcing which mainly arises from anomalous SSTs that are most persistent in the central tropical Pacific. Indeed, our results demonstrate that tropical Pacific forcing of the atmosphere like that associated with a negative phase of the PDO produces many of the pronounced atmospheric circulation anomalies observed globally during the hiatus. Tropical Pacific rainfall variations also occur on shorter time scales, including influences from the Madden-Julian Oscillation that are well established to influence the NAO[29,30] and other transients, and from El Niño events on year-to-year time scales modulated by the PDO. Consequently the exact teleconnections at any time vary substantially.

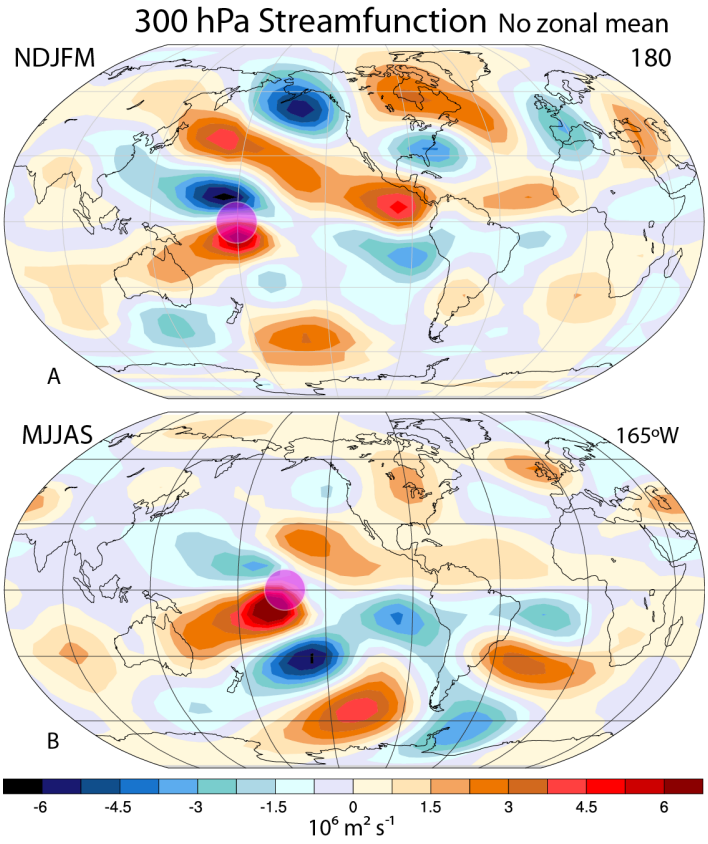

Figure 6 a,b, The streamfunction at 300 hPa response from CAM3 with circular heating on the Equator (pink circle showing the half-amplitude region) at 180_ in NDJFM(a) and 165_Wfor MJJAS (b). The zonal mean has been removed.

For instance in 2013-14 northern winter, Palmer[10] has speculated that increased greenhouse gases may have influenced the SSTs and helped trigger the substantial Rossby wave patterns of a strong ridge over the west coast of North America, a strong cold trough over the eastern United States and wet conditions over the United Kingdom. We note that the tropical Pacific rainfall during this winter featured very heavy rains near 160°E on the equator associated with "westerly wind bursts" and the developing El Niño event even though the dry region still existed in the central tropical Pacific.

Recent results[31] suggest that these influences profoundly affected the Arctic, although that study was for annual means. We are able to replicate the essence of the teleconnections using a simple forcing in a full atmospheric model, whereas a coupled model[7] did not realistically extend the patterns to the Arctic or North Atlantic. Much has been made of late about the atmosphere possibly becoming more "wavy", and claims have been made that increased waviness is associated with loss of Arctic sea ice and Arctic Amplification[32,33]. Such claims have been disputed[34,35,36]. Our results, and others[28,31,37-39] suggest an alternative hypothesis where the warmer Arctic is a consequence, not a cause, of the wavy pattern through increased exchanges of cold air from the Arctic with warmer air from lower latitudes, in association with the teleconnections across the region that originated in the tropical Pacific. More fundamentally, the reason the Arctic is a less likely source of forced atmospheric waves is because heating influences from that region are much smaller in amplitude and less persistent. Precipitation and associated latent heat anomalies are an order of magnitude less than in the tropics.

In the southern hemisphere, the tropical Pacific SST has been found to affect the Antarctic from 1979 to 2009[40], although that study did not separate the effects into the two PDO regimes, as we have done here. The change in wavetrain after 1999 (Figs. 3, 5) is mainly in winter, and again is remarkably well simulated (Fig. 6) with an idealized forcing.

There is a strong predilection for anomalous atmospheric circulation conditions mainly in the winter of each hemisphere and in the subtropics of the summer hemisphere to arise from tropical Pacific SST anomalies. These have been recognized as a dominant mode of natural interannual variability associated with ENSO, but here we focused on the inter-decadal variability that has become strongly evident recently through its manifestation as a pause in the rise of global mean temperatures. Accompanying the recent negative phase of the PDO has been striking changes in tropical and subtropical winds and ocean currents, with profound effects on OHC and sea level. Some of these aspects appear to be unique to the past decade and raise questions about whether natural internal variability itself is being altered by climate change.

Methods

Full Methods and associated references are available in the **Supplementary Information.**

References

1. Trenberth, K. E., & Fasullo, J. T. An apparent hiatus in global warming? *Earth's Future*. **1**, 19-32. doi: 10.002/2013EF000165 (2013).
2. Trenberth, K. E., Caron, J. M., Stepaniak, D.P. & Worley, S. The evolution of ENSO and global atmospheric surface temperatures *J. Geophys. Res.*, **107**, D8, 4065, 10.1029/2000JD000298 (2002).
3. Balmaseda, M. A., Trenberth, K. E., Källén, E. Distinctive climate signals in reanalysis of global ocean heat content *Geophys. Res. Lett.,* **40**, Doi: 10.1002/grl.50382 (2013).
4. Cohen, J. L., Furtado, J. C., Barlow, M., Alexeev, V. A, & Cherry J. E. Asymmetric seasonal temperature trends, *Geophys. Res. Lett*., **39**, L04705, doi:10.1029/2011GL050582. (2012).
5. Schmidt, G. A. Shindell, D. T. & Tsigaridis, K. Reconciling warming trends. *Nature Geo*, **7**, 158 – 160 doi:10.1038/ngeo2105 (2014).
6. Santer, B. et al. Volcanic contribution to decadal changes in tropospheric temperature. *Nature Geo.*, **7**, 185 – 189 doi:10.1038/ngeo2098 (2014).
7. Kosaka, Y. & Xie, S-P. Recent global-warming hiatus tied to equatorial Pacific surface cooling. *Nature*, **501**, 403-407, doi: 10.1038/nature12534 (2013).
8. Trenberth, K. E., Fasullo, J. T., & Balmaseda, M. A. Earth's energy imbalance. *J. Climate*, **27**, 3129-3144, doi: 10.1175/JCLI-D-13-00294. (2014).

9. England, M. et al. Recent intensification of wind-driven circulation in the Pacific and the ongoing warming hiatus. *Nature Clim. Change,* **4**, 222–227, doi:10.1038/nclimate2106. (2014).
10. Palmer, T. Record-breaking winters and global climate change. *Science*, **344**, 803-804 (2014).
11. Deser, C., Alexander, M. A. Xie, S.-P. & Phillips, A. S. Sea surface temperature variability: patterns and mechanisms. *Ann. Rev. Mar. Sci.*, **2010.2**, 115-143, doi:10.1146/annurev-marine-120408-151453 (2010).
12. Merrifield, M. A., Thompson, P. R. & Lander, M. Multidecadal sea level anomalies and trends in the western tropical Pacific, *Geophys. Res. Lett*., **39**, L13602, doi:10.1029/2012GL052032 (2012).
13. Holland, P. R., & Kwok, R. Wind-driven trends in Antarctic sea-ice drift. *Nature Geo.,* **5**, 872–875. doi:10.1038/ngeo1627 (2012).
14. Meehl, G. A., Arblaster, J. M., Fasullo, J. T., Hu, A. & Trenberth, K. E. Model-based evidence of deep-ocean heat uptake during surface-temperature hiatus periods. *Nature Clim. Change*, **1**, 360-364, doi: 10.1038/NCLIMATE1229 (2011).
15. Meehl, G. A., Hu, A., Arblaster, J. M., Fasullo, J. T., & Trenberth, K. E. Externally forced and internally generated decadal climate variability in the Pacific, *J. Clim.*, **26**, 7298-7310, doi:10.1175/JCLI-D-12-00548.1 (2013).
16. L'Heureux, M., Lee, S. & Lyon B. Recent multi-decadal strengthening of the Walker Circulation across the tropical Pacific. *Nature Clim. Change*, **3**, 571-576. doi:10.1038/nclimate1840 (2013).
17. Trenberth, K. E., & Guillemot, C. J. Evaluation of the atmospheric moisture and hydrological cycle in the NCEP/NCAR reanalyses. *Climate Dyn.*, **14**, 213-231 (1998).
18. Halpert, M. S. & Ropelewski, C. F. Atlas of tropical sea surface temperature and surface winds. NOAA Atlas No. 8 (1989).
19. Trenberth, K. E., & Stepaniak, D. P. Co-variability of components of poleward atmospheric energy transports on seasonal and interannual timescales. *J. Climate*, **16**, 3691-3705 (2003a).
20. Trenberth, K. E., & Stepaniak, D. P. Seamless poleward atmospheric energy transports and implications for the Hadley circulation. *J. Climate*, **16**, 3706-3722 (2003b).
21. Trenberth, K. E. Branstator, G. W., Karoly, D., Kumar, A., Lau, N-C. & Ropelewski, C. Progress during TOGA in understanding and modeling global teleconnections associated with tropical sea surface temperatures. *J. Geophys. Res.,* **103**, 14291-14324 (1998).
22. Barsugli, J. J. & Sardeshmukh, P. D. Global atmospheric sensitivity to tropical SST anomalies throughout the Indo-Pacific basin. *J. Climate*, **15**, 3427-3442 (2002).
23. Teng, H. & Branstator, G. A zonal wavenumber 3 pattern of Northern Hemisphere wintertime planetary wave variability at high latitudes. *J. Climate,* **25**, 6756–6769. doi:10.1175/JCLI-D-11-00664.1 (2012).
24. Butler, A. H., Polvani, L. M. & Deser, C. Separating the stratospheric and tropospheric pathways of El Niño–Southern Oscillation teleconnections. *Environ. Res. Lett*. **9,** 024014 doi:10.1088/1748-9326/9/2/024014 (2014).
25. Seo, K.-H., & Son, S.-W. The global atmospheric circulation response to tropical diabatic heating associated with the Madden–Julian Oscillation during northern winter. *J. Atmos. Sci.*, **69**, 79–96. doi:10.1175/2011JAS3686.1 (2012).
26. Simmons, A. J., Wallace, J. M. & Branstator, G. W. Barotropic wave propagation and instability and atmospheric teleconnection patterns. *J. Atmos. Sci.*, **40**, 1363-1392 (1983).
27. Palmer, T. N., & Mansfield, D. A. Response of two atmospheric general circulation models to sea-surface temperature anomalies in the tropical East and West Pacific. *Nature,* **310**, 483-485 (1984).
28. Lee, S., Gong, T. T., Johnson, N. C., Feldstein, S. B. & Pollard, D. On the possible link between tropical convection and the Northern Hemisphere Arctic surface air temperature change between 1958-2001. *J. Climate*, **24**, 4350-4367 (2011).
29. Cassou, C. Intraseasonal interaction between the Madden- Julian Oscillation and North
Atlantic Oscillation. *Nature*, **455**, 523-527, doi:10.1038/nature07286 (2008).
30. Lin, H., Brunet G. & Derome, J. An observed connection between the North Atlantic Oscillation and the Madden-Julian oscillation. *J. Climate*, **22**, 364-380 (2009).
31. Ding, Q., et al., Tropical forcing of the recent rapid Arctic warming in northeastern Canada and Greenland. *Nature*, **509**, 209-213, doi:10.1038/nature13260, (2014).
32. Francis, J. A. & Vavrus, S. J. Evidence linking Arctic amplification to extreme weather in mid-latitudes. *Geophys. Res. Lett*., **39**, L06801, doi:10.1029/2012GL051000 (2012).
33. Tang, Q., Zhang, X. & Francis, J. A. Extreme summer weather in northern mid-latitudes linked to a vanishing cryosphere. *Nature Clim. Change*, **4**, 45-50, doi: 10.1038/NCLIMATE2065 (2014).
34. Barnes, E. A. Revisiting the evidence linking Arctic amplification to extreme weather in midlatitudes, *Geophys. Res. Lett*., **40**, 4734–4739, doi:10.1002/grl.50880 (2013).
35. Barnes, E. A., Dunn-Sigouin, E., Masato, G. & Woollings, T. Exploring recent trends in Northern Hemisphere blocking. *Geophys. Res. Lett*., **41**, doi: 10.1002/201GL058745 (2014).
36. Wallace, J. M., Held, I. M., Thompson, D. W. J., Trenberth, K. E. & Walsh, J. E. Global warming and winter weather. *Science*, **343**, 729-730 (2014).
37. Yoo, C., Feldstein, S. & Lee, S. Impact of the Madden-Julian Oscillation (MJO) trend on the polar amplification of surface air temperature during 1979-2008 boreal winter. *Geophys. Res. Lett*., **38**, L24804, doi:10.1029/2011GL049881 (2011).
38. Lee, S. Testing of the tropically excited Arctic warming (TEAM) mechanism with traditional El Niño and La Niña. *J. Climate*, **25**, 4015-4022 (2012).
39. Lee, S., A theory for polar amplification from a general circulation perspective.
Asia-Pacific. *J. Atmos. Sci.,* **50**, 31-43. doi:10.1007/s13143-014-0024-7 (2014).
40. Ding, Q., Battisti, D. S. & Küttel, M. Winter warming in West Antarctica caused by central tropical Pacific warming. *Nat. Geo.,* **4**, 398-403, doi:10.1038/NGEO1129. (2011).

Acknowledgments. The National Center for Atmospheric Research is sponsored by the National Science Foundation. This research is partially sponsored by NASA under grant NNX09AH89G.

Author contributions

K. E. T. led the writing of the paper and conceived the study. J. T. F. and A. S. P. analyzed the data to produce most of the figures, G. B. carried out the modeling. All authors contributed to data interpretation and writing of the manuscript.

Additional information

Supplementary information is available in the online version of the paper. Reprints and permissions information is available online at www.nature.com/reprints.

Correspondence and requests for materials should be addressed to K. E. T.

Competing financial interests

The authors declare no competing financial interests.

Supplementary Information

The main datasets used include the surface temperatures from the Goddard Institute for Space Studies (GISS)[41], for precipitation GPCP v2.2 from the Global Precipitation Climatology Project[42], and for atmospheric reanalyses, ERA-Interim (ERA-I)[43]. To compute diabatic heating (Fig. 4) requires use of all levels of data every six hours[19,20] and is a major computational task.

The supplementary figures include the differences in regimes for the annual mean precipitation (Fig. S2) plotted with nonlinear contours to show the regions affected by somewhat lighter rains than possible in Fig. 3E-F. Figure S3 shows the polar map projections of the Fig. 3C-D, for sea level pressure and vector wind differences between the regimes and for the two extended seasons.

Ignoring the climatological irrotational flow, the so-called Rossby wave source[21,44] can be written as $S = -\nabla.$ $\boldsymbol{v'_d}(\zeta + f)$ where ζ is the relative vorticity, f *is* the Coriolis parameter and v'_d is the anomalous northerly divergent wind component. Separating ς into climate mean and departures, $S \cong -v'_d(\overline{\zeta}_y + \beta) - D'(\overline{\zeta} + f)$ where β is the meridional gradient of the Coriolis parameter and D is divergence. For situations involving driving by tropical precipitation, except near the subtropical jet, β is large compared to $\overline{\zeta}_y$ and D' tends to be substantial only in the vicinity of the precipitation driving.

CAM3 model experiments: The experiments are done with CAM3 at a resolution of T42 and 26 levels. Climatological SSTs are used with SST as a function of day of the year, but not a function of year. In the experiments a new heating term is included on the RHS of the thermodynamic energy equation as an extra forcing

$$\partial T/\partial t = ... + h(\lambda,\phi,\sigma) \qquad (1),$$

where $h=c*d(\lambda,\phi,\lambda_0,\phi_0,r_0)*p(\sigma)$, c is a constant, λ,ϕ,σ are latitude, longitude and the vertical normalized pressure coordinate; $p(\sigma)=sin(\pi\sigma)$ and d decreases linearly with distance from the central location at (λ_0,ϕ_0) and vanishes at a distance of r_0.

In the experiments, c = -5K day^{-1}, r_0=1.5x10^3 km; and we have placed the cooling (negative heating) at 180° or at 165°W longitude, and 0° latitude (on the equator). The imposed forcing is equivalent to a rainfall rate of about -12.8mm/day at the center of the disk or about -4.3 mm/day averaged over the disk. The response to this forcing results in a negative rainfall anomaly of similar shape that augments the imposed diabatic forcing about 30%. The net forcing (imposed plus response) has a different shape and pattern than observed but the simulated result nonetheless illustrates that negative forcing in the general region of the observed rainfall deficit (Fig. 3E-F) will generate a global circulation response with the same rich structure as the observed pattern.

The observed anomalies in precipitation reveal large areas of both positive and negative values so that the zonal mean is small. In the model experiments forced with a monopole, the zonal mean forcing gives a zonal mean response that is not small (Fig. S4). Comparison of the observed anomalies (Fig. 3) with Figs. S4 and 5, in which the zonal mean response has been removed, demonstrates this simple expedient is a good approximation to the impact of the compensating positive tropical rainfall anomalies on many mid-latitude regions.

Figure S5 presents the surface temperature anomalies in DJFM for several recent winters that were regarded as very cold in Europe, according to many media reports, see also reference (4). The three winters of particular note are illustrated in Fig. S5 and all had negative NAO values, especially 2009-10, which was 2.5 standard deviations below average. Some months were colder than others. The teleconnection patterns in Figs. 3C, 5A and 6A favor a negative NAO. The pattern (Fig. 6A) in the simple model result is not as distinctive as in Fig. 5, but nonetheless features positive values near southern Greenland and negative values over southwestern Europe.

Extra references

41. Hansen, J., Ruedy, R., Sato, M. & Lo, K. Global surface temperature change, *Rev. Geophys.,* **48**, RG4004, doi:10.1029/2010RG000345 (2010).
42. Huffman, G. J., Adler, R. F., Bolvin, D. T., Gu, G. J. Improving the global precipitation record: GPCP version 2.1, *Geophys. Res. Lett*., **36**, L17808, doi:10.1029/2009GL040000 (2009).
43. Dee, D., and Coauthors, The ERA Interim reanalysis: Configuration and performance of the data assimilation system. *Quart. J. Roy. Meteor. Soc.,* **137**, 553-597, doi: 10.1002/qj.828. (2011).
44. Sardeshmukh, P.D., & Hoskins, B.J. The generation of global rotational flow by steady idealized tropical divergence, *J. Atmos. Sci*., **45**, 1228-1251, (1988).

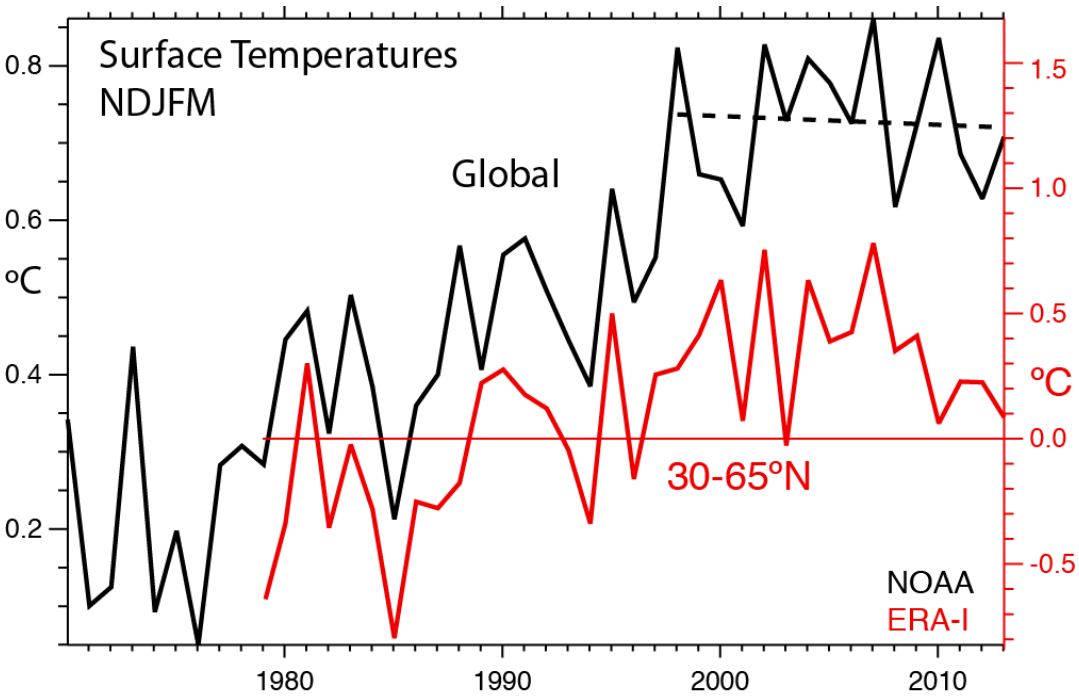

Fig. S1. For NDJFM, the global mean temperature for 1970 to 2013 and the linear trend for 1998-2013 (using NOAA data relative to the base period 1900-1999). Also shown in red are the temperature anomalies for 30-65°N relative to the mean for 1979-2013 from ERA-I data. In northern winter, when ENSO is strongest, the slight cooling trend in the 2000s exacerbates the hiatus and the coldest values are in La Niña years, however the coldest years for 30-65°N are years of negative NAO (see Figure S5).

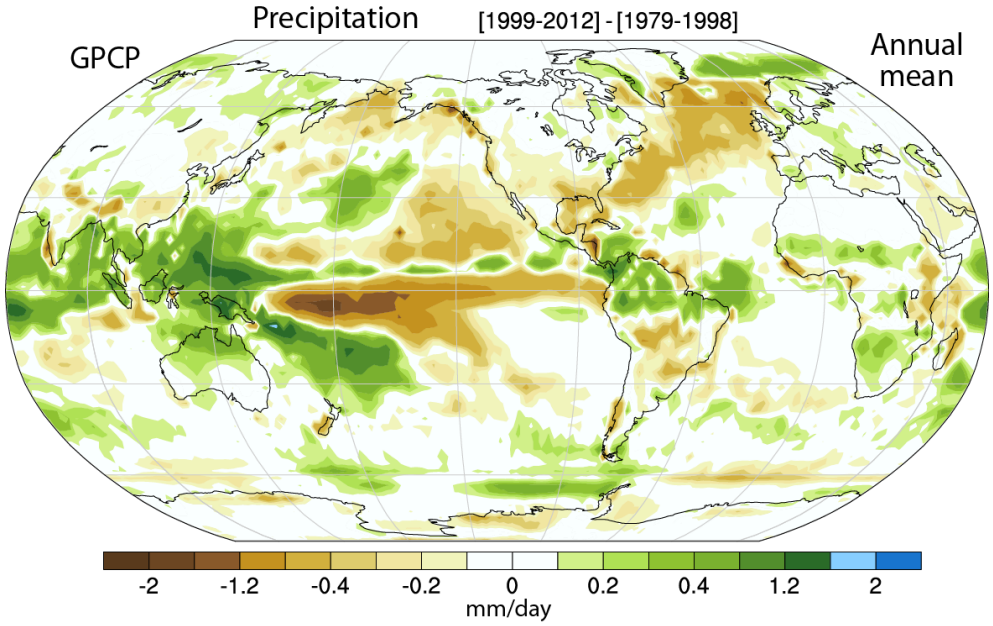

Fig. S2. Annual mean precipitation differences between 1999-2012 and 1979-1998 in mm day^{-1}. The color scale is not linear.

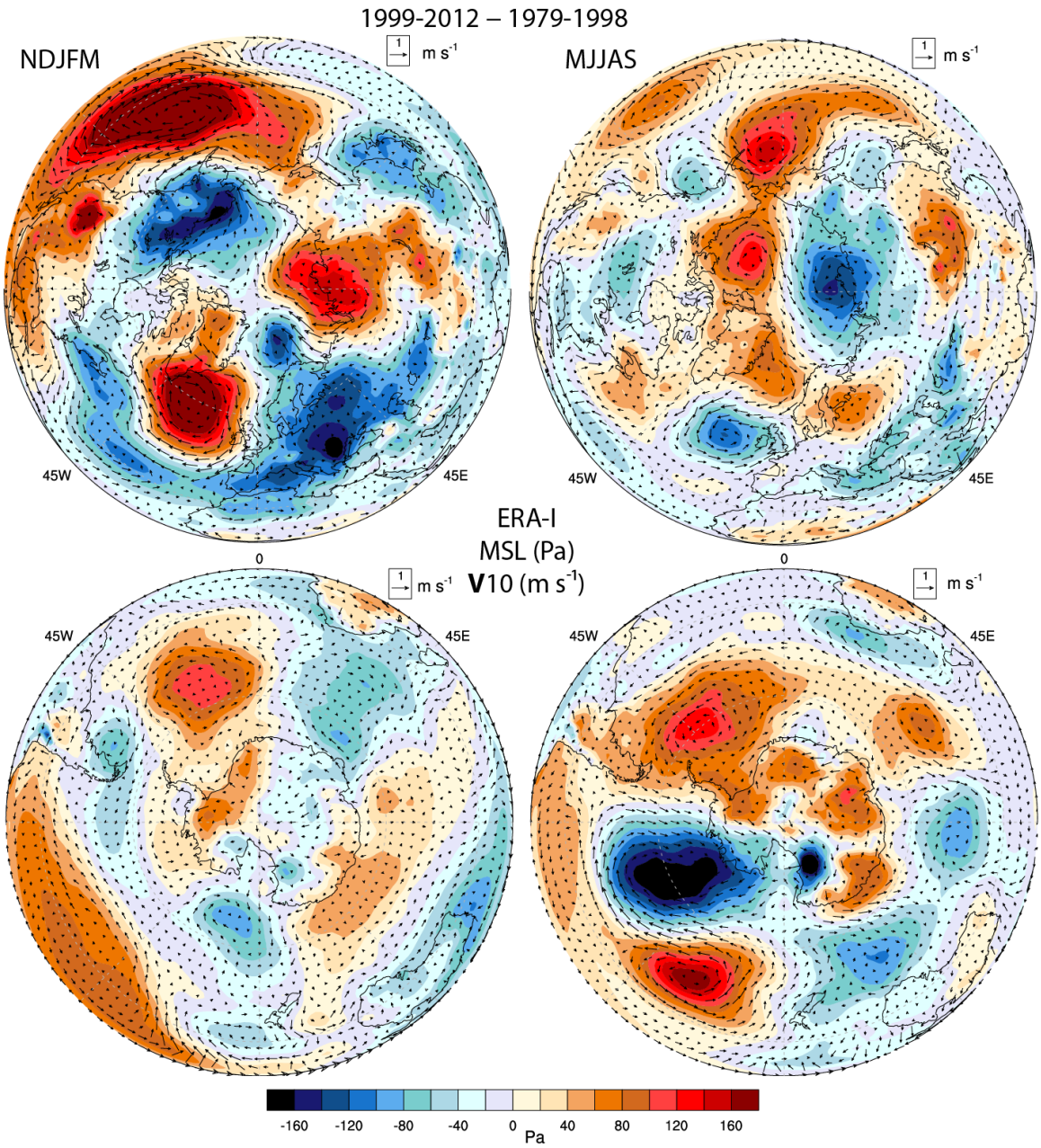

Fig. S3. Mean annual sea level pressure differences from ERA-I for 1999-2012 and 1979-1998 in Pa (colors) and for surface wind vectors (arrows) in m s^{-1} with the key at top right; for) polar stereographic projections of the Northern Hemisphere (top) and Southern Hemisphere (bottom) and for NDJFM (left) and MJJAS (right).

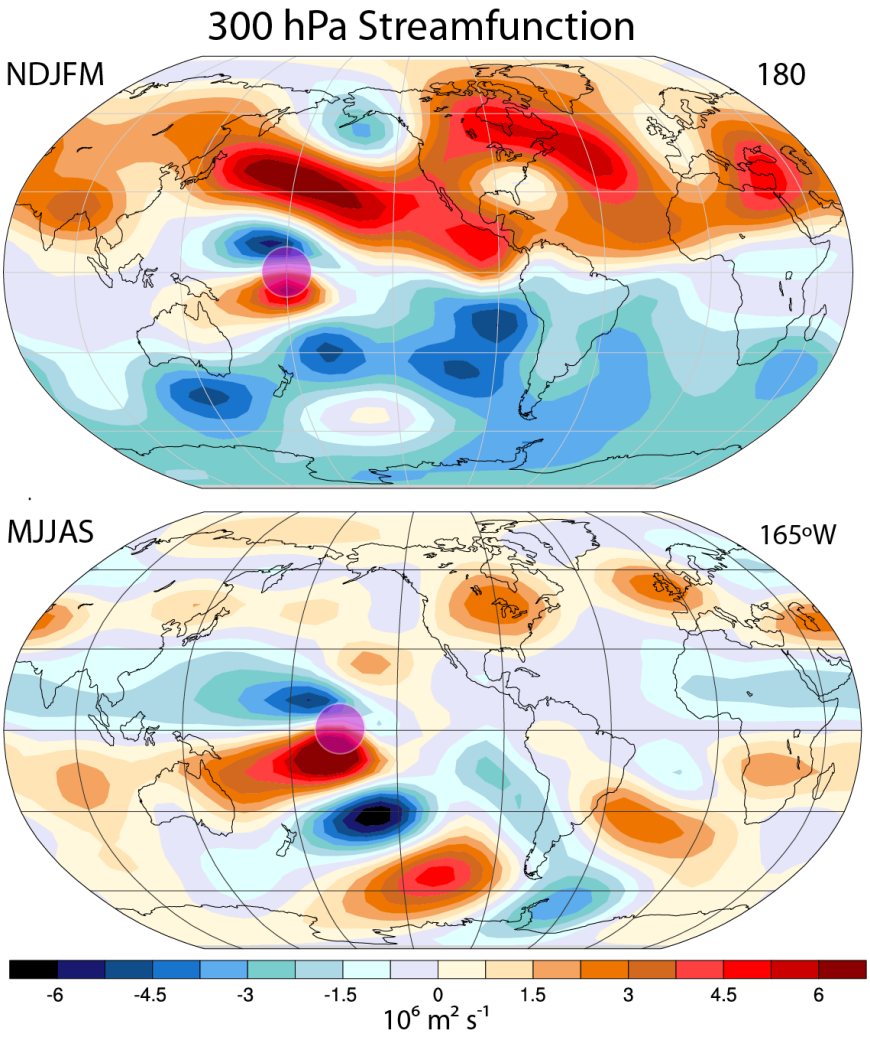

Fig. S4. The streamfunction at 300 hPa response from CAM3 with circular heating on the equator at 180° in NDJFM (top) and 165°W for MJJAS (bottom). The zonal mean is included.

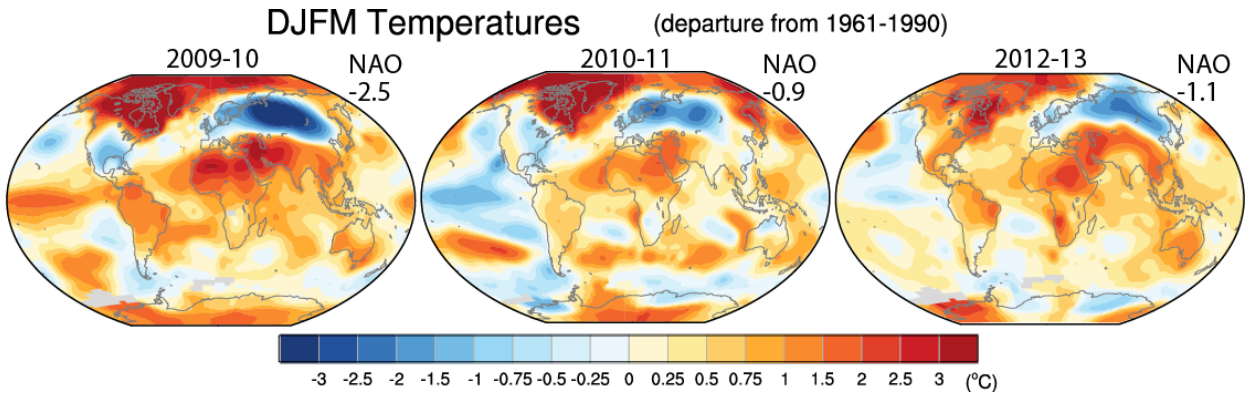

Fig. S5. Surface temperature anomalies relative to 1961-90 from GISS for the months of DJFM for northern winters of 2009-10, 2010-11, and 2012-13, which were negative NAO winters (in 2011-12 the NAO value was 1.7). The corresponding normalized NAO index value for each winter is in upper right.